Neutralized Chimeric Avidin Binding at a Reference Biosensor Surface

Santanu Ray[1], Rory T. Steven[1], Felicia Green[1], Fredrik Höök[2], Barbara Taskinen[3], Vesa P. Hytönen[3] and Alexander G. Shard[1]*

[1]Analytical Science Division, National Physical Laboratory, Teddington, UK.

[2]Applied Physics Division, Chalmers University of Technology, SE-412 96 Gothenburg, Sweden

[3] BioMediTech, University of Tampere and Fimlab Laboratories, FI-33520 Tampere, Finland.

CORRESPONDING AUTHOR FOOTNOTE. Analytical Science, National Physical Laboratory, Teddington, Middlesex, TW11 0LW (UK). email: alex.shard@npl.co.uk. Tel. +44(20)89436193.

ABSTRACT. We describe the development of a reference biosensor surface, based upon a binary mixture of oligo-ethylene glycol thiols, one of which has biotin at the terminus, adsorbed onto gold as self-assembled monolayers (SAMs). These surfaces were analyzed in detail by X-ray photoelectron spectroscopy (XPS) and secondary ion mass spectrometry (SIMS) to establish the relationship between the thiol solution composition and the surface composition and structure. We report the use of argon cluster primary ions for the analysis of PEG-thiols, establishing that the different thiols are intimately mixed and that SIMS may be used to measure surface composition of thiol SAMs on gold with a detection limit better than 1% fractional coverage. The adsorption of neutralized chimeric avidin to

these surfaces was measured simultaneously using ellipsometry and QCM-D. Comparison of the two measurements demonstrates the expected non-linearity of the frequency response of the QCM but also reveals a strong variation in the dissipation signal that correlates with the surface density of biotin. These variations are most likely due to the difference in mechanical response of neutralized chimeric avidin bound by just one biotin moiety at low biotin density and two biotin moieties at high density. The transition between the two modes of binding occurs when the average spacing of biotin molecules approaches the diameter of the avidin molecule.

Introduction

Controlling the interactions of biological molecules with surfaces is an important step for many technological developments in biotechnology and medicine.[1, 2, 3] This has been recognized for a long time and there are many elegant methods to engineer the chemistry of surfaces to prevent the binding of unwanted biomolecules and promote the selective attachment of those that are desired.[4, 5, 6] These developments are only possible through the use of highly sensitive techniques that can detect the attachment of sub-monolayer amounts of protein at interfaces.[7, 8, 9, 10, 11] These methods fall into two categories, those which have a reasonable claim to being quantitative and, those where there is still significant uncertainty about the relationship between the data they produce and physically meaningful quantities. To aid in the development of emerging techniques, we have developed a reference surface based upon well-understood thiols conjugated to biotin. These molecules can be attached in a controllable and reproducible manner to a gold surface, which is convenient because many techniques rely upon noble metal surfaces for their operation, whilst the biotin is able to capture avidin and streptavidin proteins from solution.[12] The biotin-(strept)avidin interaction is one that is commonly employed to demonstrate the performance of novel sensors.[13, 14, 15, 16, 17] It therefore makes a perfect choice as a reference system through which comparisons can be established. A future intention of this work is to translate these materials to assess the efficiency of gold nanoparticle-based sensors,[17, 18] and the establishment of a planar reference surface is an important step in progress toward this goal.

The reference surfaces described in this paper provide highly repeatable and reproducible binding of our chosen protein and we show that they also enable excellent control of the density of biotin ligands at the surface. These densities have been measured, as others have done,[19, 20] using X-ray photoelectron spectroscopy (XPS), however we demonstrate here that this technique is not sensitive enough to measure ligand densities in the dilute limit where they begin to restrict the amount of protein that can bind to the surface. We show that secondary ion mass spectrometry (SIMS) is sufficiently sensitive to extend into this dilute regime and present optimized conditions for quantitative analysis of thiol mixtures on gold surfaces. Using these conditions, and an extension to previous analyses of mixed gold-thiol secondary ions using more traditional conditions,[21] we demonstrate that our mixed thiol layers are not phase separated and that SIMS can be used to accurately measure fractional coverage below 1% of a monolayer.

We employed a novel neutralized and thermostable form of avidin, neutralized chimeric avidin (NCAvd) which has very high thermal stability, neutral pI and high affinity to biotin. NCAvd binding to gold surfaces with different biotin densities was measured with quartz crystal microbalance with dissipation (QCM-D) monitoring using a measurement cell designed for simultaneous ellipsometry measurements on the very same QCM-D sensor surface. The ellipsometry results were used to quantify the protein binding and to aid a precise correlation between the biotin density determined from the SIMS analysis and the saturated NCAvd coverage. The QCM-D data revealed a coverage dependent structural change analogous to previous observations for streptavidin and avidin binding to biotinylated supported lipid bilayers.[22, 23]

Materials and Methods

Materials and Surface Functionalization:

Biotin-PEG-SH (molecular weight. 788 Da, n=10, >95% oligomer purity) and PEG-SH (2,5,8,11,14,17,20-Heptaoxadocosane-22-thiol, molecular weight. 356.5 Da, n=6, >95% oligomer purity) were purchased from Polypure AS (Oslo, Norway) and were used without further purification. The structures of these compounds are provided in Figure 1. QCM gold-coated quartz crystals were

purchased from Biolin scientific, Sweden. Analytical grade ethanol (Fisher Scientific) was used to prepare stock solutions from the as received Biotin-PEG-SH and PEG-SH. For functionalization of gold coated crystals, a 0.5mM solution in ethanol was prepared for both Biotin-PEG-SH and PEG-SH. Mixed PEG solutions were prepared by combining the 0.5mM solutions of Biotin-PEG-SH and PEG-SH volumetrically. χ_B expresses the molar ratio of Biotin-PEG-SH to total thiol in the preparative solution. Prior to the formation of self-assembled monolayers on the gold-coated quartz crystals, the substrates were rinsed with ethanol and water and then blown dry with compressed argon, followed by 20 min of UV (ultraviolet) ozone cleaning (T10X10 ozone cleaner, UVOCS, PA, USA). The cleaned gold quartz crystals were immediately immersed in thiol solutions for 22 hours.

Neutralized Chimeric avidin (NCAvd) is based on a previously described thermostable avidin form. This novel avidin form was developed by applying charge-neutralized mutations K9E, R124H and K127E (numbering according to avidin) to previously described chimeric avidin.[24] The neutralizing mutations were designed based on structural comparison to avidin related proteins 2[25] and 4.[26] Further studies indicate that neutralizing mutations cause no changes in the thermal stability, oligomeric state or ligand binding of the protein.[27] The production and characterization of neutral chimeric avidin is detailed in the supporting information (S.1). Concentrated (10×) phosphate buffered saline (PBS) solution (pH 7.4 ± 0.1) was obtained from Fisher BioReagents. The buffer was diluted using high-purity water supplied by an Elga ultra high quality water system with resistivity =18.2 MΩ.cm (pH = 5.5 at 22°C) and was filtered using 0.2µm filters obtained from Fisher Scientific. NCAvd was supplied as 1.56 mg/ml in PBS buffer and stock solutions were diluted with PBS to 10µg/ml concentrations. All the solutions were prepared at least 12 hours before adsorption experiments and were stored in the refrigerator before removing to room temperature at least 1 hour prior to the experiment. Diluted protein solutions were never used beyond 24 hours of storage.

Methods and Instrumentation:

A quartz crystal microbalance, Q-Sense E1 (Q-sense, Biolin Scientific) with a temperature-controlled ellipsometry fluid cell, and spectroscopic ellipsometer, Woollam M2000DI (JA Woollam, NE, USA),

were used to simultaneously monitor adsorption of NCAvd. A schematic of the combined set up is shown in Figure 2. The flow rate of liquid through the fluid cell was 75 μL/min, unless otherwise stated, and the temperature 22°C. Five steps were used sequentially; the sequence was (i) water, (ii) PBS buffer, (iii) NCAvd in PBS buffer for 1 hour, (iv) PBS buffer, and (v) water. In all the steps, except (iii) the flow continued until the frequency of the QCM was visibly stable. QCM data analysis was conducted using the proprietary Q-Tools software (Q-sense, Biolin Scientific, Sweden).

Spectroscopic ellipsometry was carried out on a Woollam M2000DI (JA Woollam, NE, USA) with a fixed incidence angle of 65°. Ellipsometric data were fitted to a two-layer model using the proprietary Complete Ease Software (JA Woollam, NE, USA). In the model, the substrate was gold with optical constants determined from a clean gold substrate. The overlayer was represented by a transparent material with refractive index given by a two parameter Cauchy function, $n_{pr} = A + B/\lambda^2$, where λ is the wavelength of light and with parameters $A = 1.58$ and $B = 0.001$ μm^2 chosen to be representative of dry protein.[18] The only free parameter in the fitting is the thickness of the overlayer, T_{SE}. Dry protein thickness was converted into ellipsometric areic mass, Γ_{SE}, using $\Gamma_{SE} = \rho_{pr} T_{SE}$, where ρ_{pr} is the density of dry protein. Noting that this conversion can also be expressed by replacing ρ_{pr} with $(n_{pr} - n_w)/(dn/dc)$, where $n_w \approx 1.33$ is the refractive index of buffer and $(dn/dc) = 0.182$ cm^3/g is a good estimate of the specific refractive index increment for most proteins,[28] we use a value of $\rho_{pr} = 1.37$ g/cm^3 for consistency with these values throughout the paper.

The influence of any optical anisotropy in the windows was compensated by comparison of ellipsometric data from the same sample both inside and outside the cell. After water was introduced, the ambient refractive index in the optical model was changed to that of water to incorporate the contribution from the liquid and then fixed for the remainder of the experiment.

XPS was performed using an Axis-Ultra XPS instrument (Kratos Analytical, UK) using the selected area analysis mode with a nominal area of analysis of 55 μm and monochromated Al Kα X-rays at 1486.6 eV. The magnetic lens on this instrument provides an electron collection angle of approximately ±20° and samples were analyzed normal to the electron energy analyzer. The Al anode was operated at a

power of 450 W. Wide scans (step size 1 eV, pass energy 160 eV) and narrow scans (step size 0.1 eV, pass energy 40 eV) of the Au 4f (binding energy, BE ~84 eV), C1s (BE ~285 eV), N 1s (BE ~400 eV), S 2p (BE ~162 eV) and O 1s (BE ~532 eV) regions were acquired from three separate areas on each sample. Data were transmission function corrected and analyzed using CasaXPS (Version 2.3.15) using a Tougaard background. These are reported in the text and supporting information as atomic fractions (%), which are calculated using the Average Matrix Relative Sensitivity Factors (AMRSFs)[29] and assuming the sample to be homogeneous, as is common practice in the literature.

SIMS measurements were performed using a TOF-SIMS IV mass spectrometer (ION-TOF GmbH, Muenster, Germany) employing a pulsed analytical argon gas cluster ion beam of cluster size 5000 atoms (with a full width half maximum of approximately 50 atoms) accelerated with a potential of 20 kV. A time-averaged primary ion current of 0.04 pA was employed over a 200 × 200 μm region for a period of 400 seconds. This equates to a primary ion dose of 2.5×10^{15} ions m^{-2}, and is well below the traditional 'static' limit of 10^{17} ions m^{-2}. Data were collected in negative secondary ion mode with a cycle time for mass spectral acquisition of 200 μs, corresponding to the detection of secondary ions with mass to charge ratio = 0.5 to 3500 Da.

Results and Discussion

Analysis of sensor surfaces by XPS:

A typical XPS spectrum is provided in the supporting information S.2.1A. The elements detected on all surfaces are: gold; carbon; oxygen and; sulphur. A clear N 1s peak, arising from biotin may be identified on surfaces prepared with χ_B = 0.15 or greater. For a surface prepared at χ_B = 0.05 a weak feature is present, but barely above the background. This corresponds to an XPS detection limit of ~0.3 at% for nitrogen, which accords with the estimated detection limit for nitrogen in gold under these experimental conditions.[30] For the surface prepared at χ_B = 1, we observe two features in the S 2p region, which correspond to the thioether sulphur in biotin and the thiolate adsorbed to gold, as shown in supporting information S.2.1B. The former is significantly more intense because this sulphur is at the surface of the thiol layer and the latter is at the bottom of the layer. The intensity ratio of

thioether:thiolate R_{S2p} = 3.2 may be used as a yardstick to measure the height difference between the sulphur atoms, $d_{S\text{-}S}$, using Equation 1, the estimated electron attenuation length[31] L_{S2p} = 3.61 nm and the experimental electron take off angle φ = 0.

$$d_{S\text{-}S} = L_{S2p}\cos(\varphi)\ln(R_{S2p}) \qquad \text{Equation 1}$$

The resulting thickness, $d_{S\text{-}S}$ = 4.2 nm, provides evidence that these monolayers are well ordered and is slightly smaller than the total organic overlayer thickness, T_{org}, of 4.33 nm estimated using the relative Au 4f intensity, because $d_{S\text{-}S}$ is shorter than the full molecule and T_{org} may include any extraneous hydrocarbon contamination, which is typically an additional few Ångström.[32] T_{org} is calculated using a modified accurate equation which accounts for attenuation length differences between photoelectrons,[33] as detailed in the supporting information (S.2). The thickness of the pure PEG-SH layer prepared at χ_B = 0 is significantly smaller with an organic overlayer thickness of T_{org} = 1.28 nm. This is not due solely to the PEG-SH being a shorter molecule than Biotin-PEG-SH, but appears also to be due to a lower packing density. As shown in the supporting information (S.2), at χ_B = 1 we determine 3.6 ± 0.4 Biotin-PEG-SH molecules per nm^2, whereas at χ_B = 0 this has reduced to 2.4 ± 0.3 PEG-SH molecules per nm^2. This implies that there are attractive intermolecular forces between adsorbed Biotin-PEG-SH molecules, perhaps due to the biotin and amide moieties at the free termini. This raises concerns about the possibility that the mixed thiols are phase separated into domains on the gold surface. This question is specifically addressed in the interpretation the SIMS results presented below. It may also be tempting to try and estimate the composition of the surface from the thickness of organic overlayers; however, in light of the changes in packing density between the two pure systems, this is not possible to the required accuracy.

It is important to establish the surface density of biotin for the purpose of understanding the relationship between this and NCAvd attachment; in the high density regime XPS is ideally suited for this purpose. Using the N 1s intensity, it is possible to calculate θ_B(N), the fractional coverage of biotin on the surface normalized to the value obtained for χ_B = 1. Because the nitrogen is located close to the surface, the raw N 1s intensity is proportional to θ_B(N).[19, 20] However, to alleviate the ~5% total

intensity variations due to variations in instrumental performance and the precise positioning of samples during analysis,[34] we employ a normalization scheme, which is detailed in the supporting information (S.2).

Analysis of sensor surfaces by ToF-SIMS:

The experimental conditions for the ToF-SIMS analysis have been optimized for the analysis of thiol SAMs. The essential finding is that, by using large argon clusters (more than 1000 atoms per ion) as a primary analytical source, the negative secondary ion spectrum is considerably simplified and, at high mass, consists almost exclusively of ions of the form $Au_nM_{(n+1)}^-$, where M is a complete thiolate unit. Such results have been briefly described by Delcorte in a review of cluster beam sputtering,[35] the conditions permit simple data analysis without interference from fragments and gold-sulphur clusters observed using traditional atomic primary ions.[36, 37, 38] It has previously been noted that in a binary thiol overlayer there are three possible AuM_2^- secondary ions and the detection of an ion containing dissimilar thiols indicates an intimate mixture of the two at the surface.[21] Furthermore, if the relative secondary ion yields are constant it is possible to analyse the relative secondary ion intensities of such secondary ion series to obtain both the composition and local structure of mixed systems, an exemplary case being the secondary ion series $(3M\text{-}O)^+$ from poly(lactide-co-glycolide).[39]

In the SIMS spectra of these surfaces, we observe the secondary ions AuP_2^-, where P is PEG-S^- at ~908 Da, AuB_2^-, where B is Biotin-PEG-S^- at ~1771 Da, and $AuBP^-$ at ~1340 Da. Unfortunately, the use of large argon clusters results in a poor mass resolution due to the spread in arrival times of clusters of slightly different size. However, the assignments are unambiguous and the spectra very clear as shown in Figure 3. The intensities of these ions are obtained by summing the counts under the full isotopic envelope of each peak and subtracting the background (due to metastables and low intensity interferences) to obtain I_i for each spectra, where i = 0, 1 or 2 depending upon the number of Biotin-PEG-S^- units in the ion $AuB_iP_{(2-i)}^-$. The background intensity, from very low intensity secondary ions and metastables, at these positions are measured from the pure thiol layers formed using χ_B = 0 and 1. The normalized intensities, I_i^*, for the series are obtained through Equation 2.

$$I_i^* = \frac{I_i}{\sum I_i}$$ Equation 2

Now, if the relative partial yields for these three ions are identical at all compositions, and the two thiols are distributed randomly on the surface, we should expect these intensities to follow a binomial distribution such that $I^*_0 = (1- \theta_B)^2$, $I^*_1 = 2(1- \theta_B)\ \theta_B$ and $I^*_2 = \theta_B^2$. In Figure 4 a comparison is made between the normalized intensities and the binomial predictions using $\theta_B(N)$ for three compositions. The excellent correspondence confirms that the relative partial yields for these three ions are closely similar and that, at least within the scale length of the primary ion impact crater (~10 nm) the two thiols are intimately mixed. If the thiols were phase-separated into their components, then the mixed ion $AuBP^-$ could only be formed if a primary ion impact occurred on the boundary of the two phases. Because it is observed at the predicted intensities, this is strong evidence for a uniform mixture.

Furthermore, because of the identity in the relative partial ion yields across the AuM_2^- ion series, it becomes simple to estimate the fractional composition from the observed intensities in SIMS, $\theta_B(S)$, using Equation 3.

$$\theta_B(S) = 0.5I_1^* + I_2^*$$ Equation 3

This enables us to measure the compositions of the mixed thiol monolayers for compositions lower than the detection limit of XPS at $\theta_B \sim 0.03$. The detection limit and precision of SIMS is constrained by the presence of a background in the data, which exceeds the signal for the $AuBP^-$ secondary ion at $\chi_B = 0.005$, or $\theta_B(S) = 0.003$; this represents a reasonable estimate of the limitations of this method: it is an order of magnitude more sensitive than XPS. For these systems with low biotin coverage we find that $\theta_B(S) \approx 0.5\ \chi_B$, implying that the rate of attachment of PEG-SH is approximately twice that of Biotin-PEG-SH, and that we may use a description of the form shown in Equation 4 to estimate the relationship between surface and solution molar fractions.

$$\theta_B = \chi_B/(2 - \chi_B)$$ Equation 4

Composition of the sensor surfaces:

Figure 5 summarises the results of the analysis of our surfaces. In Figure 5A the total organic thickness determined by XPS, T_{org}, is plotted as a function of surface composition, χ_B, demonstrating a monotonic increase from $\chi_B = 0$ to $\chi_B = 1$. The curve is not linear and this results from a combination of packing effects, different thiol sizes and the relationship between solution and surface composition. Figure 5B shows the thiol composition of the overlayer, θ_B, as a function of surface composition, χ_B. The XPS results, θ_B(N), are imprecise but accurate (in the sense that XPS is a well understood quantitative method with known uncertainties) and the SIMS results, θ_B(S), are very precise but of accuracy which can only be validated by the XPS measurements. The excellent agreement between the two methods shown in this plot is a validation of the SIMS approach at values of θ_B where XPS is able to detect nitrogen. Under the assumption that this remains valid at lower θ_B, we also show an expanded view in Figure 5C, where the reliance is solely on the SIMS data. Plotted in both Figure 5B and 5C are the output of Equation 4, which provides a reasonable description of θ_B up to $\chi_B = 0.5$. Later we show that NCAvd adsorption is identical for all $\chi_B > 0.15$ ($\theta_B > 0.08$), therefore we calculate θ_B using Equation 4 in the later text and introduce no significant error.

Overview of QCM and ellipsometry during NCAvd adsorption:

Figure 6 displays, as black lines, the frequency and dissipation shifts of the seventh overtone (F7 and D7) during NCAvd adsorption onto a surface coated only with Biotin-PEG-SH, $\theta_B = 1$. The trace shows the following features: after exchanging water with buffer there is a rapid change in resonant frequency and dissipation due to the different density and viscosity of the buffer from that of pure water. Thereafter, the typical features of protein adsorption are observed: on exchange to the protein solution, a drop in resonant frequency can be observed, consistent with efficient protein binding to the biotin-containing sensor surface. Some transient changes can also be observed in the dissipation trace, the origin of which will be discussed later. The frequency appears to stabilize after approximately 10 minutes however, there is a continual and barely perceptible decrease in frequency which continues for at least 10 more minutes. We show later that QCM is insensitive to protein adsorption in the high coverage regime and this apparent stabilization is therefore somewhat deceptive. After exchange of the

protein solution with buffer we observe no change in frequency or dissipation, indicating that the protein layer is essentially irreversibly bound to the sensor. Finally, the buffer is exchanged for water to enable drying prior to XPS analysis.

After exchanging water with buffer there is a rapid decrease in QCM resonant frequency and an increase in dissipation, attributed to the different density and viscosity of the buffer from that of pure water. When water replaces the buffer after protein adsorption is complete, there is a change in dissipation and frequency roughly of the same magnitude and opposite to that observed for the exchange from water to buffer.

The bold red line in Figure 6 shows the protein areic mass derived from the spectroscopic ellipsometry data, Γ_{SE}, from the same experiment. We observe a change in Γ_{SE} of ~0.15 mg m^{-2} after the exchange of water to buffer is complete, presumably due to either the slight difference in refractive index between these liquids, or the association of ions with the surface. After the addition of protein we observe a rapid increase in Γ_{SE} over the same period as the change in frequency in QCM-D, then a slow rise over the course of ~20 minutes. We also display as a dotted red line the ellipsometric data for a surface coated only with PEG-SH, $\theta_B = 0$, showing no detectable protein adsorption. The QCM-D data for these surfaces are equally uneventful.

First note that the ellipsometry trace in Figure 6 shows two distinct features when water is exchanged for buffer and then back again toward the end of the experiment. This is correlated with a near total loss of detected intensity in the ellipsometer and explained by refractive index of water and buffer being sufficiently different to deflect the path of light during the exchange in the cell. There is no loss of intensity in ellipsometry during the buffer to NCAvd solution exchange and this measurement is therefore only affected by changes at the sensor surface. However, due to fluid exchange effects in the cell, an analysis of binding kinetics is replaced by a comparison of the bound mass and structural differences of the adsorbed film that can be deduced from combined QCM-D and ellipsometry data.

Ellipsometric measurement of the total amount of NCAvd adsorbed:

We turn first to the ellipsometry data, which are expected to provide the best quantitative estimate of the amount of adsorbed protein. In Figure 7 the total change in areic mass, $\Gamma_{SE}(max)$ is plotted as a function of θ_B. The graph demonstrates the remarkably consistent performance of this system, with repeat experiments at θ_B = 1 and 0.15 providing closely similar values. For θ_B larger than 0.01, the values of $\Gamma_{SE}(max)$ are, within experimental error, identical at 2.53 ± 0.03 mg m^{-2}. This is consistent with the 2.54 ± 0.30 mg m^{-2} inferred from ρ_{pr} = 1.37 g/cm^3 and the change in T_{org} of 1.86 ± 0.20 nm from the XPS analysis of sensors before and after protein adsorption, see Figure 7 and supporting information. This observation is contradictory to previous works using Biotin-PEG-SH and PEG-SH modified gold surfaces where a maximum adsorption was observed at $\theta_B \approx 0.2$,[19, 20] however these studies were performed with Biotin-PEG-SH containing only 2 or 3 ethylene glycol repeat units, severely restricting the ability of the SAM layer to deform and accommodate protein binding. Here, there are 10 ethylene glycol repeat units in the molecular monolayer, which appears to solve this complication and enables a repeatable response which is robust to small changes in surface coverage.

In the $\theta_B > 0.15$ regime, the maximum NCAvd adsorption is limited by the size of NCAvd itself, and there are more than sufficient biotin ligands on the surface to facilitate binding in any location. We may compare T_{org} to the thickness expected from the crystallographic size: ~5 nm (see Figure 1C) and infer that the protein layer contains ~40% protein and ~60% water by volume. For θ_B smaller than 0.01, the values of $T_{SE}(max)$ are linear with θ_B, this is shown more clearly in the inset of Figure 7, in this regime the biotin molecules are sparsely located on the surface and the maximum NCAvd adsorption is limited by their areic density. The intercept of the linear fits to both the low θ_B and high θ_B regimes shown in Figure 7 is at $\theta_B \sim 0.01$ and the inverse of this should correspond to the product of the packing density of thiols at this composition (~2.6 molecules per nm^2, see supporting information) and the surface area occupied by an NCAvd molecule. From this we can infer that NCAvd occupies an area of ~40 nm^2 on the surface which is higher than the expected footprint of ~33 nm^2. This implies a reasonably close packing of molecules on the surface with approximately three quarters of the surface occupied by adsorbed NCAvd. This is higher than the random sequential adsorption ‘jamming limit’, which results

in coverage only slightly larger than half.[40] Furthermore, since the biotin moieties are randomly distributed across the surface, at $\theta_B \sim 0.01$ and lower the majority of NCAvd molecules must be bound only through one biotin link since the average spacing of biotin ligands in this regime is larger than the distance between the two available NCAvd binding sites.

QCM response as a function of the amount of NCAvd adsorbed:

In Figure 8A we compare the change in QCM frequency, $\Delta F7$, to the ellipsometric areic mass, Γ_{SE}, during the adsorption process. Data from surfaces with θ_B = 1, 0.08, 0.01, 0.005 and 0.0025 are displayed, but are difficult to distinguish as they exhibit the same behavior. The response of the frequency shift to adsorbed amount is clearly non-linear and displays monotonically declining sensitivity as the coverage of NCAvd increases. In the low coverage regime, the additional mass of entrained water surrounding isolated molecules is well documented, as is the role of water entrapped within the protein itself.[22, 28] From the initial and final gradients of these curves, it is clear that the sensitivity of QCM to a fractional increase in protein coverage decreases by an order of magnitude from low to high coverage. Therefore, a quantitative analysis of protein attachment is rather difficult using this technique on its own. The curve shown in Figure 8A, however, is well behaved and can be rationalized through a comparison of the estimated areic mass of attached protein, which is measured by ellipsometry, Γ_{SE}, and the areic mass of protein and liquid mechanically coupled to the layer, measured by the QCM ($\Gamma_{QCM} = -C\Delta F7/7$), in which we use the mass sensitivity coefficient C = 0.1806 ± 0.0015 mg m^{-2} Hz^{-1} for a 5 MHz quartz crystal.[22] The fractional mass of trapped liquid can be calculated as $H = 1 - (\Gamma_{SE} / \Gamma_{QCM})$, and a plot of this against Γ_{SE} is provided in Figure 8B for data from θ_B =1. The result is a highly linear correlation, similar to previous studies of avidin and streptavidin adsorption, where various models have been employed to explain these results.[22, 41] Here, it is sufficient to state that the fractional trapped liquid for isolated molecules tends to H_0 = 0.86 (~14% by mass protein, or ~10% by volume) and for a nearly complete layer is $H \sim 0.5$ (~50% by mass protein, or ~40% by volume). This

latter value is consistent with the estimate made from the crystallographic dimensions of the protein and the ellipsometric thickness.

QCM reveals structural differences in bound NCAvd:

Figure 8C shows the changes in QCM-D dissipation against equivalent ellipsometric thickness for different values of θ_B. For $\theta_B > 0.15$ there are no substantial differences in these data and, of these, only $\theta_B = 1$ is shown for clarity. All sensor surfaces demonstrate a rise in dissipation at the initiation of adsorption. At high θ_B, this rise reaches a maximum and then decreases, the position of the maximum in Γ_{SE} increasing as θ_B decreases. The magnitudes of changes in dissipation correlate in a similar fashion and it is clear that at, for example, $\Gamma_{SE} = 0.5$ mg m^{-2}, there must a significant structural difference between the adsorbed layers formed at high θ_B and those formed at low θ_B. Höök *et al* and Bingen *et al* both observed similar effects for streptavidin adsorption, to biotinylated supported lipid bilayers, without exploring the relationship to biotin coverage,[22, 23] and Bingen *et al* ascribed this to mechanical stabilization. A later analysis of colloidal particle adsorption by Tellechea *et al* demonstrated that such behavior for large particles can arise from hydrodynamic effects and, in such cases, plotting the ratio of dissipation change to frequency change against frequency results in a linear correlation which is not observed for uniform viscoelastic film growth. Furthermore, the extrapolated intercept of such a plot with the frequency change axis can provide a reasonable estimate of the mass of a complete layer of particles from which the diameter can be inferred.[42]

In Figure 9 we display such plots for the data acquired here and it is clear from these plots that there is at least a fourfold difference in dissipation between the surfaces prepared with different biotin densities. We find linearity for surfaces with $\theta_B = 0.01$ and lower. The extrapolated intercepts correspond to $\Gamma_{QCM} \approx 5.8$ mg m^{-2}, which indicates a thickness, or NCAvd diameter of ~4.2 nm for NCAvd using a dry protein density of $\rho_{pr} = 1.37$ g/cm^3. A close packed layer of proteins would contain a substantial fraction of water both in and between the molecules, having a lower density and larger thickness than calculated here. Therefore this is quite a reasonable result and matches well with the expected value of

~5 nm for NCAvd. However, at high biotin densities the analogous plot is non-linear since the dissipation change returns to zero within the data, *i.e.* prior to maximum binding being reached. The intercepts in these cases return unphysically small diameters for NCAvd and it is clear that additional effects are occurring which result in a different mechanical response to the low biotin coverage case.

A plausible explanation for these observations is that the attachment of NCAvd to the surface is restricted to being through only one biotin moiety when the spacing of biotin ligands is larger than the diameter of the NCAvd molecule whereas, at high biotin density, NCAvd is capable of binding to the surface through two biotin moieties. We call these modes of attachment respectively monovalent and divalent binding. In consideration of the distance between binding sites on the NCAvd molecule the transition should occur close to $\theta_B \sim 0.02$, as indeed is observed and, as θ_B reduces, the fractional population of monovalently bound NCAvd should increase. We therefore expect the data in Figure 9 to lie between two boundaries defined by the QCM response to divalent NCAvd and the response to monovalent NCAvd binding. These limiting cases should be reasonably represented by the data given by $\theta_B = 1$ for divalent binding and the data and extrapolation given by $\theta_B = 0.0025$ for monovalent binding. The data indeed fall between these boundaries, although it is not possible at this stage to attempt a quantitative analysis of the fractional population of monovalently bound NCAvd with any certainty because the cause of the anomolous QCM response to divalent binding is still unclear. The effect may arise from a number of factors including: stronger mechanical coupling of the sensor to bound NCAvd molecules compared to monovalent binding; cross-linking and stiffening of the PEG layer by divalent binding or; surface association of bound NCAvd molecules in the divalent case (island formation). Nevertheless, these results demonstrate that one may control, detect and possibly quantify the fractional population of monovalent and divalent NCAvd molecules and this ability could provide insight into the mechanisms of avidin association and dissociation at sensor surfaces.

Conclusions

We have developed highly stable and reproducible reference surfaces based on thiol-modified gold and using the biotin-avidin interaction. These have been measured with XPS and SIMS to provide

detailed information on the composition and structure of the self-assembled thiol monolayer. Through the use of a novel primary ion source, argon clusters, we demonstrate that very clean and useful spectra from thiols on gold may be obtained that can be employed both to demonstrate that thiols are not significantly phase separated and to measure low surface concentrations of thiol, approaching one molecule in a thousand. These analyses show that an exquisite control of biotin surface density may be achieved.

The simultaneous use of ellipsometry and QCM to measure NCAvd adsorption to these reference surfaces demonstrates that the frequency change in QCM, whilst highly sensitive to the adsorption of protein, has a coverage dependent sensitivity that changes by at least an order of magnitude. This means that QCM frequency changes should be used with extreme caution when trying to understand, for example, the kinetics and mechanisms of protein adsorption. The adsorption of NCAvd to this surface and under the conditions employed here appears to show two distinct modes of binding, which can be clearly detected in the dissipation signal of the QCM-D, and we ascribe these to the difference in mechanical response of this system to NCAvd bound through either one or two biotin moieties.

ACKNOWLEDGMENT. This work forms part of the Chemical and Biological programme of the National Measurement System of the UK Department of Business, Innovation and Skills and with additional funding from the European Union through the European Metrology Research Programme (EMRP) project BioSurf. The EMRP is jointly funded by the EMRP participating countries within EURAMET and the European Union. The Academy of Finland is acknowledged for financial support. We thank David Castner, University of Washington, Dmitri Petrovykh, International Iberian Nanotechnology Laboratory and Jennifer Shumaker-Parry, University of Utah for providing invaluable advice on the development of the reference surface and Ralph Richter, CIC biomaGUNE, San Sebastian for helpful advice and comments. The authors are deeply indebted to one of the reviewers for providing insight into fluid exchange phenomena in the liquid cell used in this study.

SUPPORTING INFORMATION AVAILABLE. Supporting information contains: details of the preparation and characterization of the NCAvd protein; XPS results and a general method for measuring organic film thicknesses on gold using XPS and; a justification for the use of only one QCM-D overtone in the paper. This information is available free of charge via the Internet at http://pubs.acs.org/.

REFERENCES

1. Malmsten, M. Studies of serum protein adsorption at phospholipid surfaces in relation to intravenous drug delivery. *Colloids and Surfaces A: Physicochemical and Engineering Aspects* **1999,** *159* (1), 77-87.
2. Castner, D. G.; Ratner, B. D. Biomedical surface science: Foundations to frontiers. *Surface Science* **2002,** *500* (1-3), 28-60.
3. Kasemo, B. Biological surface science. *Current Opinion in Solid State & Materials Science* **1998,** *3* (5), 451-459.
4. Denis, F. A.; Hanarp, P.; Sutherland, D. S.; Gold, J.; Mustin, C.; Rouxhet, P. G.; Dufrene, Y. F. Protein adsorption on model surfaces with controlled nanotopography and chemistry. *Langmuir* **2002,** *18* (3), 819-828.
5. Camarero, J. A. Recent developments in the site-specific immobilization of proteins onto solid supports. *Biopolymers* **2008,** *90* (3), 450-458.
6. Huang, N.-P.; Michel, R.; Voros, J.; Textor, M.; Hofer, R.; Rossi, A.; Elbert, D. L.; Hubbell, J. A.; Spencer, N. D. Poly(l-lysine)-*g*-poly(ethylene glycol) Layers on Metal Oxide Surfaces: Surface-Analytical Characterization and Resistance to Serum and Fibrinogen Adsorption. *Langmuir* **2001,** *17* (2), 489 - 498.
7. Geddes, N. J.; Pachinger, E. M.; Furlong, D. M.; Ebara, Y.; Okahata, Y.; Than, K. A.; Edgar, J. A. Piezoelectric crystal for the detection of immunoreactions in buffer solutions. *Sensors and Actuators B: Chemical* **1994,** *17* (2), 125-131.
8. Stenberg, E.; Persson, B.; Roos, H.; Urbaniczky, C. Quantitative determination of surface concentration of protein with surface plasmon resonance using radiolabeled proteins. *Journal of Colloid and Interface Science* **1991,** *143* (2), 513-526.
9. Malmsten, M. Ellipsometry studies of fibronectin adsorption. *Colloids and Surfaces B: Biointerfaces* **1995,** *3* (6), 371-381.
10. Elwing, H. Protein absorption and ellipsometry in biomaterial research. *Biomaterials* **1998,** *19* (4-5), 397-406.
11. Pasche, S.; De Paul, S. M.; Voros, J.; Spencer, N. D.; Textor, M. Poly(l-lysine)-graft-poly(ethylene glycol) Assembled Monolayers on Niobium Oxide Surfaces: A Quantitative Study of the Influence of Polymer Interfacial Architecture on Resistance to Protein Adsorption by ToF-SIMS and in Situ OWLS. *Langmuir* **2003,** *19* (22), 9216-9225.
12. Häussling, L.; Ringsdorf, H.; Schmitt, F.; Knoll, W. Biotin-functionalized self-assembled monolayers on gold: surface plasmon optical studies of specific recognition reactions. *Langmuir* **1991,** *7* (9), 1837-1840.
13. Iqbal, M.; Gleeson, M. A.; Spaugh, B.; Tybor, F.; Gunn, W. G.; Hochberg, M.; Baehr-Jones, T.; Bailey, R. C.; Gunn, L. C. Label-Free Biosensor Arrays Based on Silicon Ring Resonators and High-Speed Optical Scanning Instrumentation. *Ieee Journal of Selected Topics in Quantum Electronics* **2010,** *16* (3), 654-661.

14. Duan, X.; Li, Y.; Rajan, N. K.; Routenberg, D. A.; Modis, Y.; Reed, M. A. Quantification of the affinities and kinetics of protein interactions using silicon nanowire biosensors. *Nature Nanotechnology* **2012,** *7* (6), 401-407.
15. Escobedo, C.; Vincent, S.; Choudhury, A. I. K.; Campbell, J.; Brolo, A. G.; Sinton, D.; Gordon, R. Integrated nanohole array surface plasmon resonance sensing device using a dual-wavelength source. *Journal of Micromechanics and Microengineering* **2011,** *21* (11).
16. Zhang, H.; Pang, W.; Marma, M. S.; Lee, C.-Y.; Kamal-Bahl, S.; Kim, E. S.; McKenna, C. E. Label-free detection of protein-ligand interactions in real time using micromachined bulk acoustic resonators. *Applied Physics Letters* **2010,** *96* (12).
17. Oh, E.; Hong, M. Y.; Lee, D.; Nam, S. H.; Yoon, H. C.; Kim, H. S. Inhibition assay of biomolecules based on fluorescence resonance energy transfer (FRET) between quantum dots and gold nanoparticles. *Journal of the American Chemical Society* **2005,** *127* (10), 3270-3271.
18. Bell, N. C.; Minelli, C.; Shard, A. G. Quantitation of IgG protein adsorption to gold nanoparticles using particle size measurement. *Analytical Methods* **2013,** *5* (18), 4591-4601.
19. Perez-Luna, V. H.; O'Brien, M. J.; Opperman, K. A.; Hampton, P. D.; Lopez, G. P.; Klumb, L. A.; Stayton, P. S. Molecular recognition between genetically engineered streptavidin and surface-bound biotin. *Journal of the American Chemical Society* **1999,** *121* (27), 6469-6478.
20. Ballav, N.; Terfort, A.; Zharnikov, M. Fabrication of Mixed Self-Assembled Monolayers Designed for Avidin Immobilization by Irradiation Promoted Exchange Reaction. *Langmuir* **2009,** *25* (16), 9189-9196.
21. Stranick, S. J.; Atre, S. V.; Parikh, A. N.; Wood, M. C.; Allara, D. L.; Winograd, N.; Weiss, P. S. Nanometer-scale phase separation in mixed composition self-assembled monolayers. *Nanotechnology* **1996,** *7* (4), 438-442.
22. Bingen, P.; Wang, G.; Steinmetz, N. F.; Rodahl, M.; Richter, R. P. Solvation Effects in the Quartz Crystal Microbalance with Dissipation Monitoring Response to Biomolecular Adsorption. A Phenomenological Approach. *Analytical Chemistry* **2008,** *80* (23), 8880-8890.
23. Höök, F.; Ray, A.; Nordén, B.; Kasemo, B. Characterization of PNA and DNA immobilization and subsequent hybridization with DNA using acoustic-shear-wave attenuation measurements. *Langmuir* **2001,** *17* (26), 8305-8312.
24. Hytönen, V. P.; Määttä, J. A.; Nyholm, T. K.; Livnah, O.; Eisenberg-Domovich, Y.; Hyre, D.; Nordlund, H. R.; Hörhä, J.; Niskanen, E. A.; Paldanius, T. Design and construction of highly stable, protease-resistant chimeric avidins. *Journal of Biological Chemistry* **2005,** *280* (11), 10228-10233.
25. Hytönen, V. P.; Määttä, J. A.; Kidron, H.; Halling, K. K.; Hörhä, J.; Kulomaa, T.; Nyholm, T. K.; Johnson, M. S.; Salminen, T. A.; Kulomaa, M. S. Avidin related protein 2 shows unique structural and functional features among the avidin protein family. *BMC biotechnology* **2005,** *5* (1), 28.
26. Hytönen, V. P.; Nyholm, T. K.; Pentikäinen, O. T.; Vaarno, J.; Porkka, E. J.; Nordlund, H. R.; Johnson, M. S.; Slotte, J. P.; Laitinen, O. H.; Kulomaa, M. S. Chicken avidin-related protein 4/5 shows superior thermal stability when compared with avidin while retaining high affinity to biotin. *Journal of Biological Chemistry* **2004,** *279* (10), 9337-9343.
27. Taskinen, B.; Zauner, D.; Lehtonen, S. I.; Koskinen, M.; Thomson, C.; Kähkönen, N.; Kukkurainen, S.; Määttä, J. A.; Ihalainen, T. O.; Kulomaa, M. Switchavidin: reversible biotin-avidin-biotin bridges with high affinity and specificity. *Bioconjugate Chemistry* **2014**.
28. Vörös, J. The Density and Refractive Index of Adsorbing Protein Layers. *Biophysical Journal* **2004,** *87* (1), 553 - 561.
29. Seah, M. P.; Gilmore, I. S.; Spencer, S. J. Quantitative XPS I. Analysis of X-ray photoelectron intensities from elemental data in a digital photoelectron database. *Journal of Electron Spectroscopy and Related Phenomena* **2001,** *120* (1-3), 93-111.
30. Shard, A. G. Detection limits in XPS for more than 6000 binary systems using Al and Mg Ka X-rays. *Surface and Interface Analysis* **2014,** *46* (3), 175-185.
31. Seah, M. P. Simple universal curve for the energy-dependent electron attenuation length for all materials. *Surface and Interface Analysis* **2012,** *44* (10), 1353-1359.

32. Techane, S.; Baer, D. R.; Castner, D. G. Simulation and Modeling of Self-Assembled Monolayers of Carboxylic Acid Thiols on Flat and Nanoparticle Gold Surfaces. *Analytical Chemistry* **2011,** *83* (17), 6704-6712.
33. Shard, A. G. A Straightforward Method For Interpreting XPS Data From Core-Shell Nanoparticles. *Journal of Physical Chemistry C* **2012,** *116* (31), 16806-16813.
34. Ray, S.; Shard, A. G. Quantitative Analysis of Adsorbed Proteins by X-ray Photoelectron Spectroscopy. *Analytical Chemistry* **2011,** *83* (22), 8659-8666.
35. Delcorte, A.; Cristaudo, V.; Lebec, V.; Czerwinski, B. Sputtering of polymers by keV clusters: Microscopic views of the molecular dynamics. *International Journal of Mass Spectrometry* **2014,** *370* (0), 29-38.
36. Tarlov, M. J.; Newman, J. G. Static secondary ion mass spectrometry of self-assembled alkanethiol monolayers on gold. *Langmuir* **1992,** *8* (5), 1398-1405.
37. Sun, L. M.; Gardella, J. A. Oxidation-assisted secondary ion mass spectrometry methodology to quantify mixed alkylthiol self-assembled monolayers on gold: Applications to competitive chemical adsorption. *Langmuir* **2002,** *18* (24), 9289-9295.
38. Graham, D. J.; Ratner, B. D. Multivariate analysis of TOF-SIMS spectra from dodecanethiol SAM assembly on gold: Spectral interpretation and TOF-SIMS fragmentation processes. *Langmuir* **2002,** *18* (15), 5861-5868.
39. Shard, A. G.; Volland, C.; Davies, M. C.; Kissel, T. Information on the monomer sequence of poly(lactic acid) and random copolymers of lactic acid and glycolic acid by examination of static secondary ion mass spectrometry ion intensities. *Macromolecules* **1996,** *29* (2), 748-754.
40. Rabe, M.; Verdes, D.; Seeger, S. Understanding protein adsorption phenomena at solid surfaces. *Advances in Colloid and Interface Science* **2011,** *162* (1), 87-106.
41. Carton, I.; Brisson, A. R.; Richter, R. P. Label-free detection of clustering of membrane-bound proteins. *Analytical Chemistry* **2010,** *82* (22), 9275-9281.
42. Tellechea, E.; Johannsmann, D.; Steinmetz, N. F.; Richter, R. P.; Reviakine, I. Model-independent analysis of QCM data on colloidal particle adsorption. *Langmuir* **2009,** *25* (9), 5177-5184.

FIGURES.

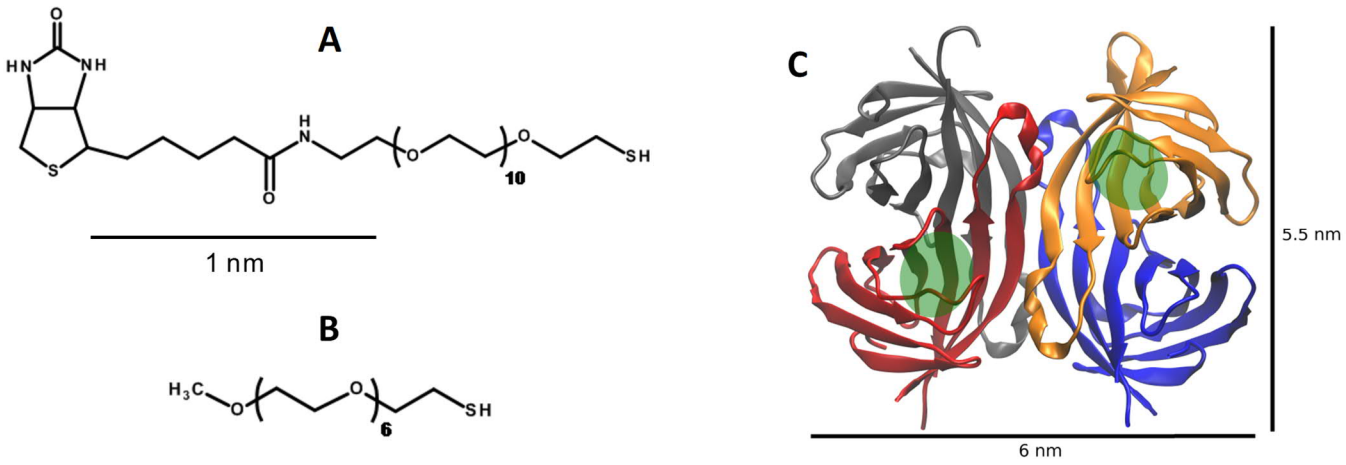

Figure 1. The structures of (A) Biotin-PEG-SH (~6 nm long), (B) PEG-SH (~3 nm long) and (C) NCAvd, which has crystallographic dimensions approximately 6 nm×5.5 nm×5 nm (Protein Data Bank id 3mm0, representing a closely related protein form), two of the four biotin binding sites are marked with green circles. The protein is expected to bind to the surface through one or two binding sites with the shortest axis perpendicular, *i.e.* occupying an area of 33 nm^2 with a thickness of 5nm.

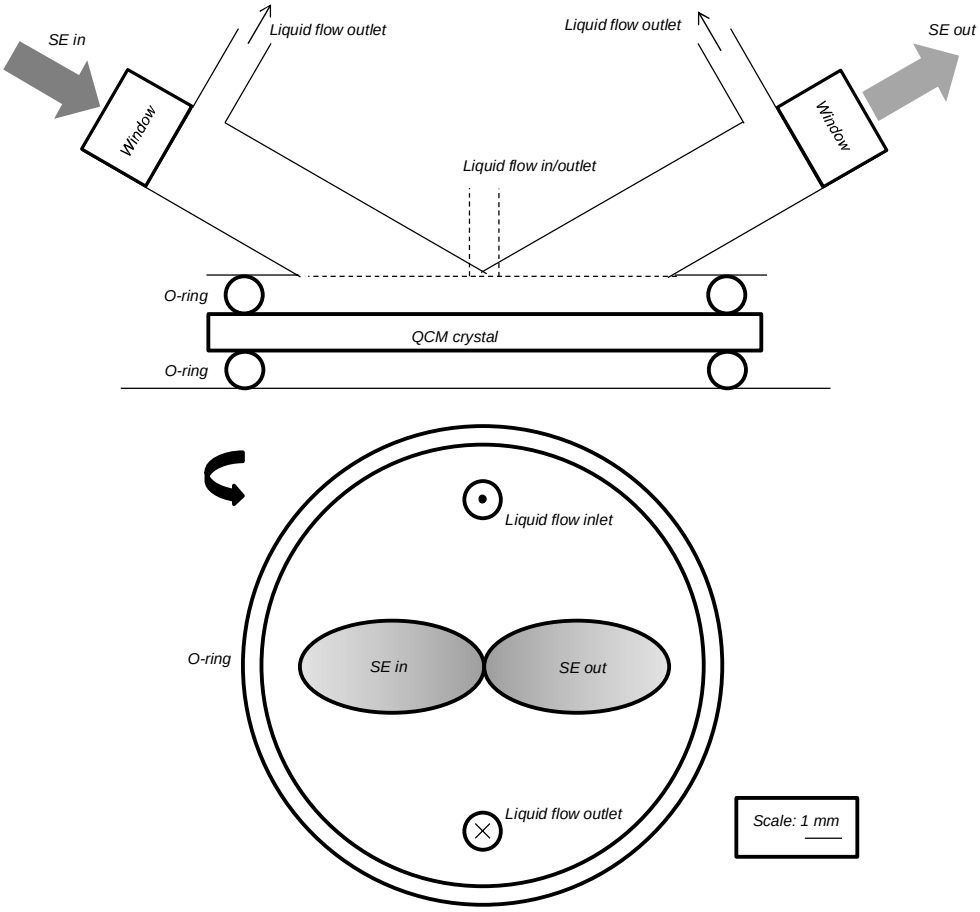

Figure 2. Diagram of the QCM/SE liquid cell showing the liquid flow inlet and outlets, and ellipsometry windows (SE). The upper figure shows a cross-section of the cell from the side. Dotted lines in the top figure indicate surfaces outside the plane of the cross-section. The QCM crystal sits between two o-rings and the arms and windows allow *in-situ* ellipsometry. The arms are filled with liquid and there are two liquid outlets along the arms to prevent bubbles at the windows. The lower figure is a plan view of the surface indicated by dotted lines in the upper figure.

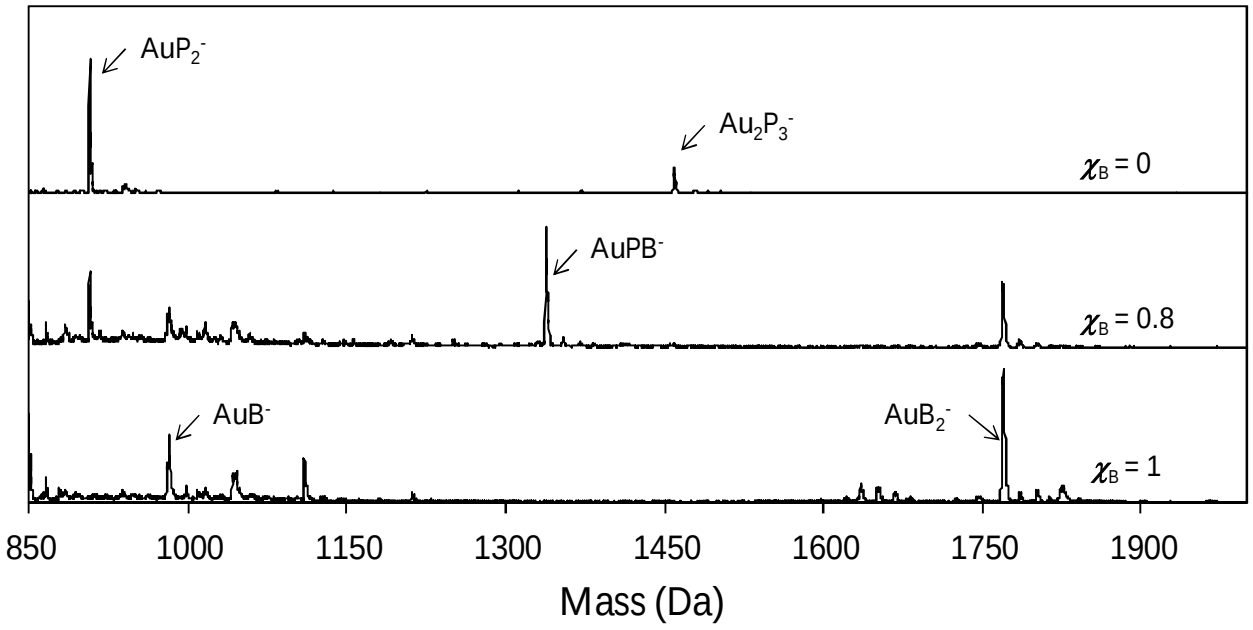

Figure 3. Argon cluster ToF-SIMS spectra of the AuM_2^- region for three surfaces on a linear intensity scale, identifying the three secondary ions used for analysis in this work: AuP_2^-; $AuPB^-$ and AuB_2^-. Other secondary ions are observed; however, these spectra are remarkably free of interfering ions.

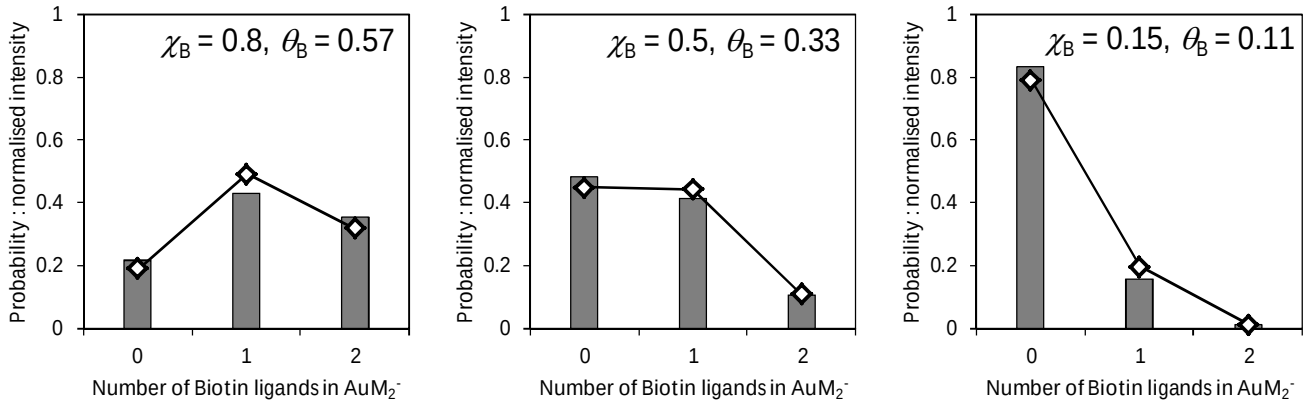

Figure 4. The distribution of intensities between the AuM_2^- series of secondary ions, the prediction from $\theta_B(N)$ using a binomial distribution are shown as diamonds (◇) and the normalized measured intensities $I^*(i)$ as grey bars.

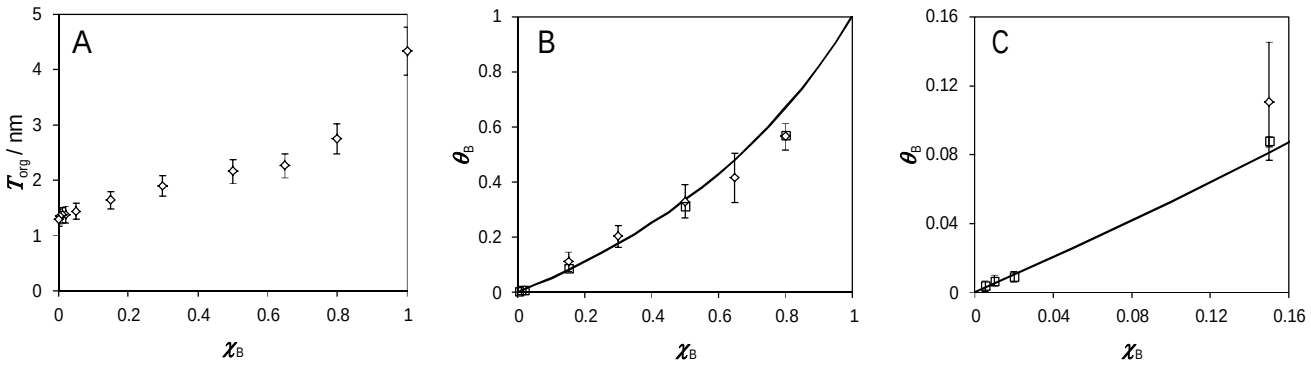

Figure 5. (A) The thickness of organic overlayer on gold, T_{org}, as a function of the solution composition, χ_B. Error bars represent the 10% uncertainty in electron attenuation length, L. The precision of the results are better than 0.05 nm. (B) The estimated fractional coverage of biotin, θ_B, as a function of the solution composition, χ_B. XPS results from the N1s intensity θ_B(N) are plotted as diamonds (◇) along with their standard deviations as error bars. SIMS results from the AuM_2^- intensities, θ_B(S), are similarly plotted as squares (□). The line shows Equation 4. (C) Expanded region of (B) in the region below the XPS detection limit for nitrogen.

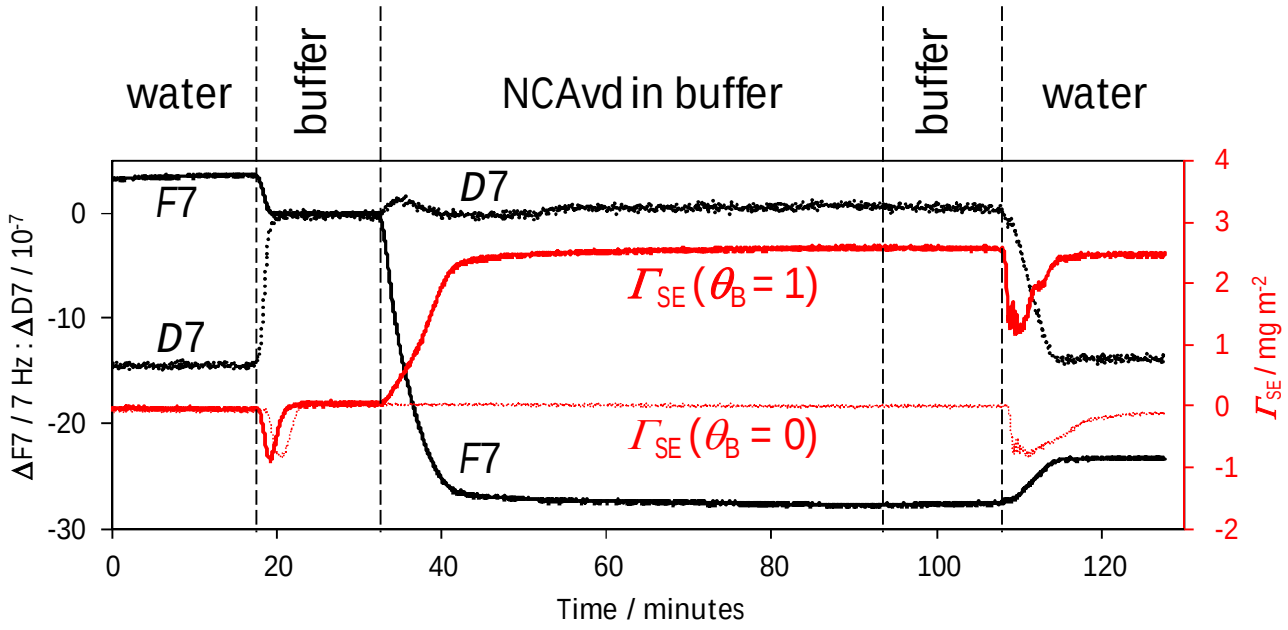

Figure 6. QCM-D (black, left hand axis) and ellipsometry data (red, right hand axis) acquired during the adsorption of NCAvd to a sensor surface prepared from Biotin-PEG-SH, $\chi_B = 1$. For comparison, the ellipsometry data, Γ_{SE}, for a sensor surface prepared from PEG-SH, $\chi_B = 0$, is shown as a dotted red line. The approximate times when changes were made to the liquid flowing into the cell are marked as vertical dashed lines. All data are referenced to the measurement made in buffer before the start of NCAvd adsorption.

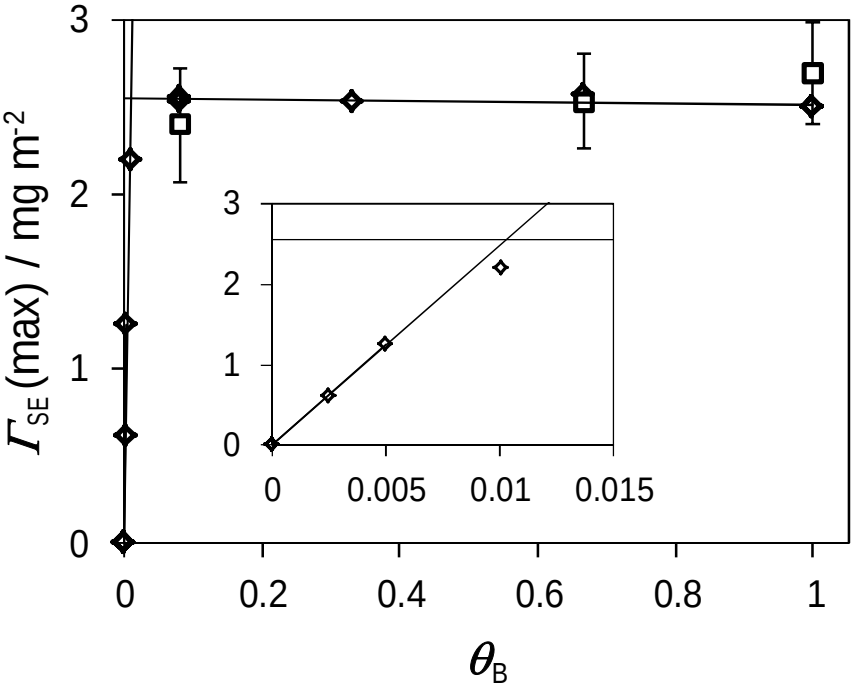

Figure 7. The maximum areic mass of protein adsorbed, Γ_{SE}(max) (◇) measured during adsorption of NCAvd to sensor surfaces prepared from mixtures of Biotin-PEG-SH and PEG-SH as a function of θ_B, the biotin surface fraction. The inset shows an expanded view of the region where $\theta_B \sim 0.01$. Lines are linear fits to two regimes: $\theta_B > 0.01$ and $\theta_B < 0.01$. For comparison, the areic mass of NCAvd inferred from XPS organic overlayer thicknesses, T_{org}, (□) are plotted, with uncertainties as error bars, on the same axes.

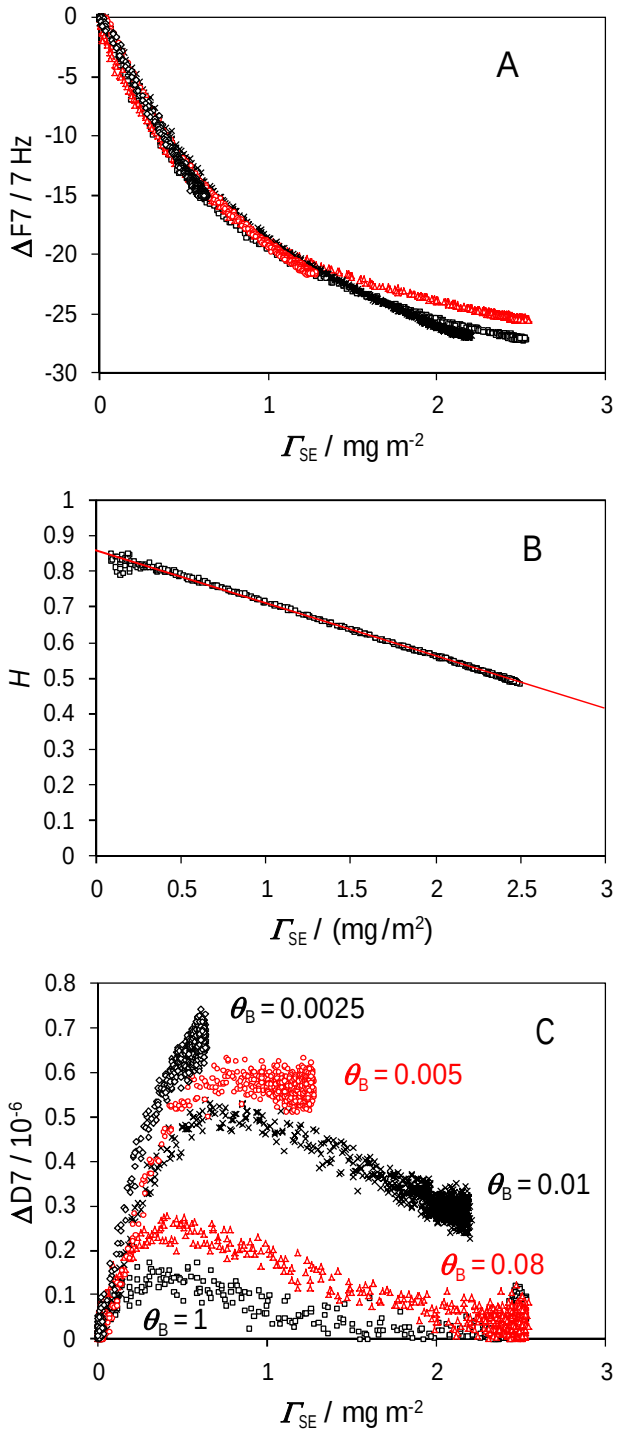

Figure 8. The correlation of QCM-D data with spectroscopic ellipsometry. Frequency change (A) and dissipation (C) are plotted against Γ_{SE} for selected sets of data from sensor surfaces prepared with θ_B =1 (□), 0.08 (△, red), 0.01 (×), 0.005 (○, red) and 0.0025 (◇). (B) The estimated fractional mass of trapped liquid, H, for χ_B =1, is plotted against the estimated areic mass of dry NCAvd from ellipsometry, Γ_{SE}. The red line shows a linear fit with intercept H_0 = 0.86.

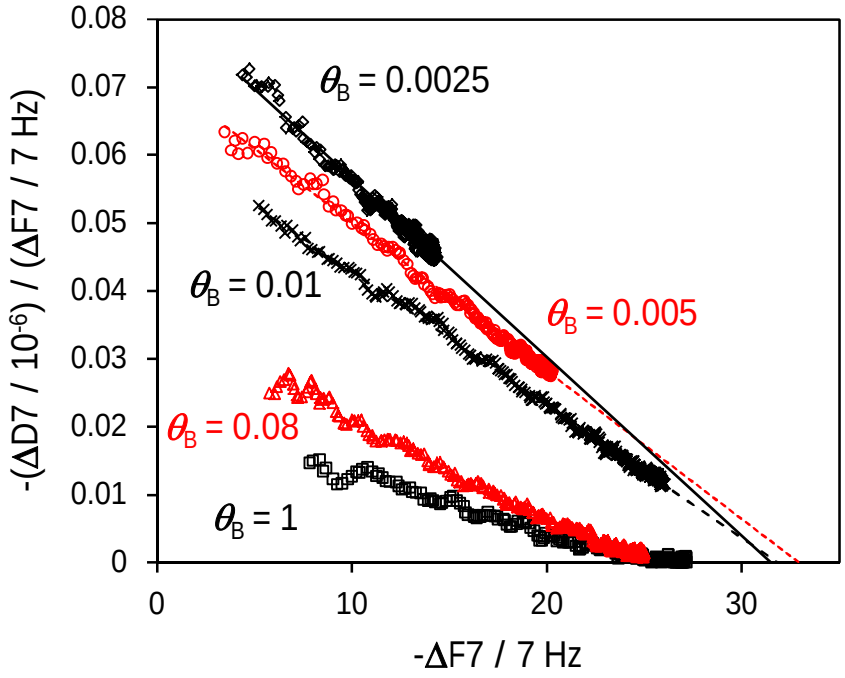

Figure 9. The ratio of QCM dissipation to QCM frequency plotted against QCM frequency change from sensor surfaces prepared with θ_B =1 (□), 0.08 (△, red), 0.01 (×), 0.005 (○, red) and 0.0025 (◇) demonstrates two different modes of NCAvd binding. Due to noise in the dissipation signal, the data are truncated at the low frequency end and smoothed using a running five point mean for clarity. The extrapolated intercepts for NCAvd adsorbing on surfaces with low θ_B are displayed.

ToC graphic

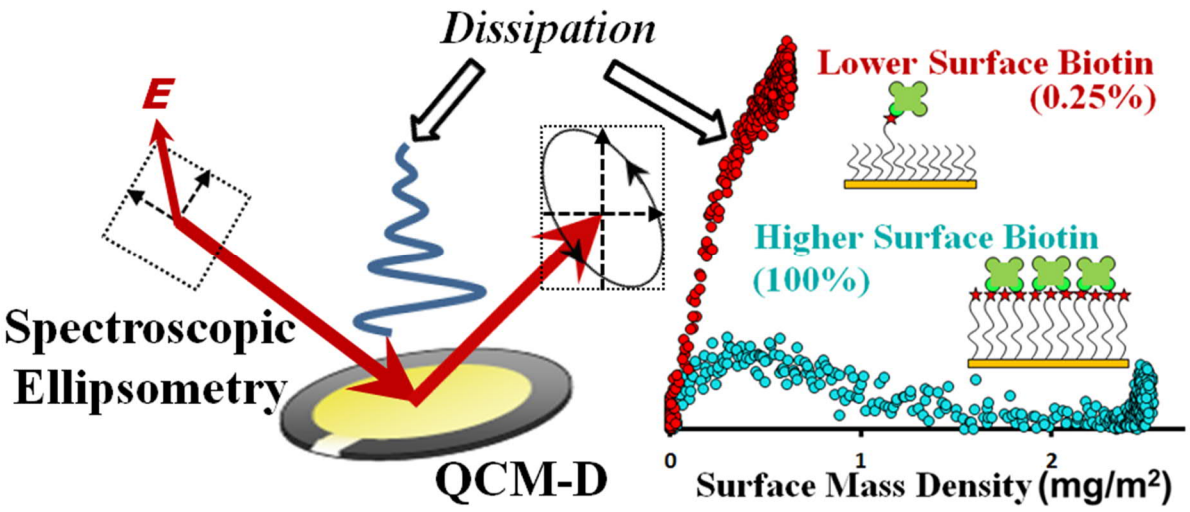
Dissipation
E
Spectroscopic
Ellipsometry
QCM-D
Lower Surface Biotin
(0.25%)
Higher Surface Biotin
(100%)
0
1
2
Surface Mass Density (mg/m²)